High gradient magnetic particle separation in viscous flows by 3D BEM

J. Ravnik & M. Hriberšek

Computational Mechanics
Solids, Fluids, Structures, Fluid-Structure Interactions, Biomechanics, Micromechanics, Multiscale Mechanics, Materials, Constitutive Modeling, Nonlinear Mechanics, Aerodynamics

ISSN 0178-7675
Volume 51
Number 4

Comput Mech (2013) 51:465-474
DOI 10.1007/s00466-012-0729-3

Springer

Comput Mech (2013) 51:465–474
DOI 10.1007/s00466-012-0729-3

ORIGINAL PAPER

High gradient magnetic particle separation in viscous flows by 3D BEM

J. Ravnik · M. Hriberšek

Received: 9 February 2012 / Accepted: 5 May 2012 / Published online: 24 May 2012

Abstract The boundary element method was applied to study the motion of magnetic particles in fluid flow under the action of external nonuniform magnetic field. The derived formulation combines the velocity-vorticity resolved Navier–Stokes equations with the Lagrange based particle tracking model, where the one-way coupling with fluid phase was considered. The derived algorithm was used to test a possible design of high gradient magnetic separation in a narrow channel by computing particles trajectories in channel flow under the influence of hydrodynamic and magnetic forces. Magnetic field gradient was obtained by magnetization wires placed outside of the channel. Simulations with varying external magnetic field and flow rate were preformed in order to asses the collection efficiency of the proposed device. We found that the collection efficiency decreases linearly with increasing flow rate. Also, the collection efficiency was found to increase with magnetic field strength only up a saturation point. Furthermore, we found that high collection efficiently is not feasible at high flow velocity and/or at weak magnetic field. Recommendation for optimal choice of external magnetic field and flow rate is discussed.

Keywords Boundary element method · Lagrangian particle tracking · High gradient magnetic separation · Magnetic spheres · Velocity-vorticity

J. Ravnik (✉) · M. Hriberšek
Faculty of Mechanical Engineering, University of Maribor,
Smetanova 17, 2000 Maribor, Slovenia
e-mail: jure.ravnik@uni-mb.si

M. Hriberšek
e-mail: matjaz.hribersek@uni-mb.si

1 Introduction

Nano and micro particles with magnetic properties are increasingly gaining interest in several fields of science, like life sciences, natural sciences, medicine or engineering sciences. In biomedicine, for example, they are used for magnetic separation of labelled cells and other biological entities [8,29], for therapeutic drug, gene, radionuclide delivery [2], in radio frequency methods for the catabolism of tumours via hyperthermia or for contrast enhancement agents for magnetic resonance imaging applications.

The dimensions of magnetic nanoparticles are smaller than or comparable to the size of cells, viruses or proteins, enabling them to interact with biological agents directly and thereby providing a controllable means of tagging and addressing specific cells. Due to magnetic properties, the movement of the particles may be manipulated with an external magnetic field gradient [13]. Several studies dealing with synthesis of such particles have been performed [25]. Iron oxides, i.e. magnetite Fe_3O_4 and maghemite γ-Fe_3O_4, are the most frequently used because of their generally suitable magnetic properties and biological compatibility.

Furthermore, there exists a growing clinical need to remove nanoparticles from the human body. Kaminski and Rosengart [9] proposed a high gradient magnetic separator device (HGMS) suitable for biomedical applications. Combination of functionalized magnetic particles and a magnetic separation device makes it possible to remove blood-borne biological agents from the human body. This paper focuses on the performance of a HGMS device used to remove magnetic particles from the flow. For a medical application, such a device would receive blood from the body by an extracorporeal circulation. After removal of the magnetic particles from the blood in the device, the blood would return to the body.

Magnetic separators for biological separations have been extensively studied in recent years. The effect of magnetic forces on particles in flow was considered by Yang et al. [30], who studied motions of magnetic nanospheres under the magnetic field in the rectangular microchannel. Nakamura et al. [12] developed a quadrupole magnetic flow sorter to facilitate high-throughput binary cell separation. Pekas et al. [15] developed a fully integrated micromagnetic particle diverter and microfluidic system. Particles are diverted via an external uniform magnetic field perturbed at the microscale by underlying current straps. The resulting magnetic force deflects particles across a flow stream into one of the two channels at a Y-shaped junction. Furlani [6] performed an analytical analysis of the transport and capture of magnetic micro/nanoparticles in a magnetophoretic microsystem that consists of an array of integrated soft-magnetic elements embedded beneath a microfluidic channel. Ritter et al. [22] studied a magnetic drug targeting system, utilizing HGMS principles, using FEMLAB simulations. They proposed using a ferromagnetic wire placed at a bifurcation point inside a blood vessel and an externally applied magnetic field, to magnetically guide magnetic drug carrier particles through the circulatory system and then to magnetically retain them at a target site.

Conventional HGMS systems [31,11,4,27,17] make use of designs where the magnetisable wires are submerged in the fluid. In this paper, we study a separator, with magnetisable wires placed outside of the separation channel. Such a design can be used for biomedical applications since direct interactions between the blood components and wires, which would lead to flow obstructions, is avoided.

In order to accurately describe hydrodynamics of flows with particles in the context of the Euler–Lagrangian formulation, the computationally most affordable approach is the description of a particle as a rigid sphere, that interacts with the fluid phase. At the same time, however, the particle occupies the same volume as the fluid. The interaction of both phases is in general modelled by a point source approach. The flow of the continuous phase is computed by means of a standard CFD approach. Lagrangian particle tracking has a superior spatial accuracy, and allows different phenomena to be modelled and computed accurately, e.g. heat and mass transfer from the particles or accurate incorporation of drag and lift forces. In general, the computational cost of the method is proportional to the particle concentration.

A boundary element method (BEM) based numerical algorithm is proposed for simulation of laminar flow of dilute suspension of small magnetic particles in a HGMS device. Several BEM based algorithm have been proposed for viscous and non-viscous flows [1,7,5,24,23]. Our method is based on the velocity–vorticity formulation of Navier–Stokes equations in Eulerian framework coupled with a Lagrangian particle tracking algorithm. A combined single domain and domain decomposition approach is employed to reduce the computational and memory requirements of the algorithm, [21,28].

Efficient algorithms for Lagrangian particle tracking in fluid flow are an ongoing research topic. Recently, Cohen Stuart et al. [26] developed a method tackling unstructured grids. In our work, as a starting point, the earlier work by Ravnik et al. [19] was chosen, where a 2D flow simulation was coupled with an explicit Lagrangian particle tracking algorithm. The flow algorithm was extended to a 3D geometry in Ravnik et al. [21] and in this work coupling with particle tracking is presented. In order to realistically capture the particle response to fluid flow structures, a full one-way coupling approach is implemented. The particles are moving due to the action of gravity, buoyancy, drag, pressure gradient and added mass forces. When the fluid flows through the area of a non-uniform external magnetostatic field, the resulting magnetophoretic force working on the particles is also considered. Since numerical simulation of dilute suspensions is the main target of this work, the coupling between the two phases is a one-way action of the fluid on the particles.

2 Problem description

We consider separation of polystyrene magnetic spheres flowing in water in a HGMS unit. The magnetic spheres produced by Micromod Inc. (Germany) are considered. The spheres have a hydrodynamic diameter of $d_\mathrm{p} = 1.7\,\mu\mathrm{m}$. The spheres contain 12.45 % of magnetite ($\rho_\mathrm{m} = 5{,}000\ \mathrm{kg/m^3}$) and 88.55 % polystyrene ($\rho_\mathrm{ps} = 1047\ \mathrm{kg/m^3}$). These values were obtained by means of dynamic laser scattering in a zeta potential analyser and thermogravimetry analysis by Chen et al. [3]. Spheres are considered to be uniformly dispersed in water at temperature 20 °C (viscosity $\nu = 1.01\ \mathrm{mm^2/s}$ and density $\rho_\mathrm{f} = 998\ \mathrm{kg/m^3}$).

The separator unit consists of 10 cm long square cross section ($0.75 \times 0.75\,\mathrm{mm^2}$) channel. On the top and on the bottom of the channel two stainless steel 430 wires of diameter 0.5 mm are placed. Figure 1 presents the problem setup.

The unit is placed into a homogenous external magnetic field produced by parallel rectangular NdFeB magnets.

Average mean flow velocities in the channel up to 8 cm/s are considered. This corresponds to flow rate of 162 ml/h and to a Reynolds number of $Re = 59.4$. Due to the small Reynolds number value, the flow is laminar and steady. At the inlet the flow is assumed to be fully developed and the magnetic spheres are homogenously distributed. Dilute suspensions of magnetic spheres in water are considered, thus the interaction between particles is neglected. Furthermore, one-way coupling between particles and flow is considered. In this model, the movement of particles is affected by the flow, while the flow itself is not affected by the particles.

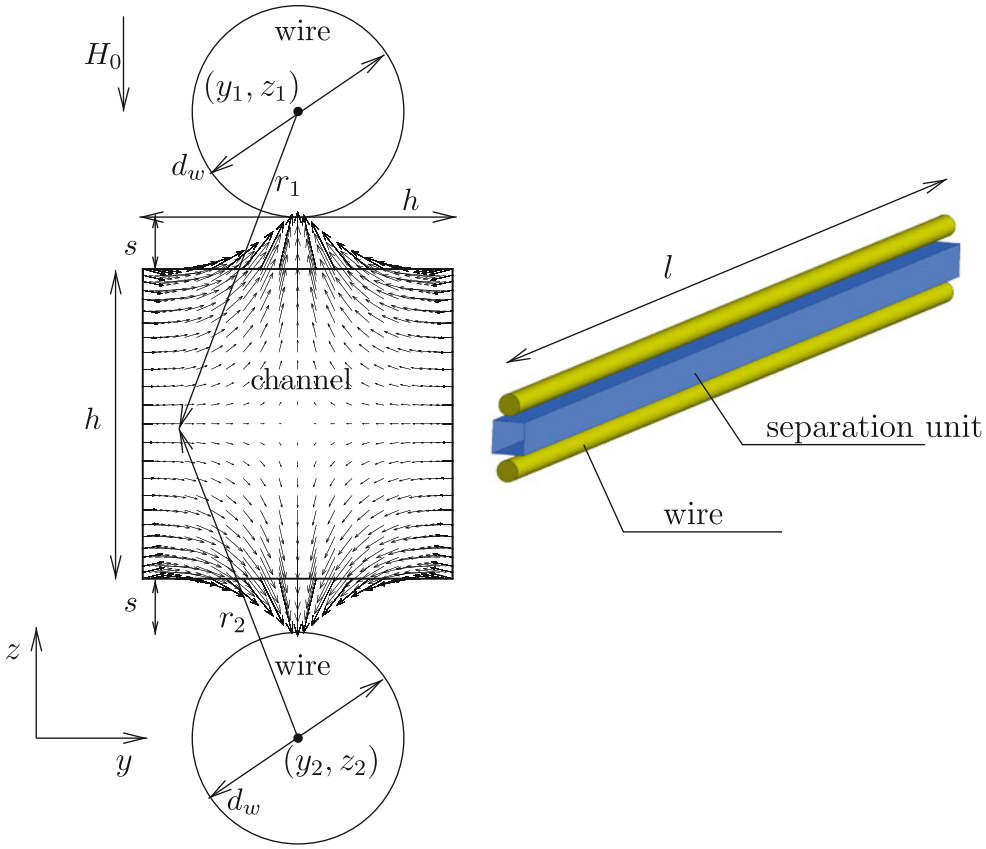

Fig. 1 Separation channel cross section with magnetic force vectors displayed (*left*) and side view (*right*). Two magnetized stainless steel 430 wires are shown. Channel height and width $h = 0.75$ mm, $s = 0.125$ mm, wire diameter $d_w = 0.5$ mm. Length of the unit is $l = 10$ cm

Due to a very high aspect ratio of the channel (0.75 mm width versus 10 cm length) only a shorter 4.5 mm section of the channel is simulated using periodic boundary conditions. Values of velocity and vorticity at the outlet are copied back to the inlet plane. In the same manner, particle positions at the outlet are used as inlet positions for simulation of the next segment of the channel.

3 Fluid flow computation

The flow in the magnetic separation unit is considered to be Newtonian, incompressible, fully developed and steady. Considering medical applications, removal of magnetic spheres from blood stream is foreseen to take place with flow rates between 10 and 162 ml/h [3]. These flow rates correspond to average flow velocities from $u_0 = 0.5$ cm/s to $u_0 = 8$ cm/s and Reynolds number values from $Re = \frac{u_0 h}{\nu} = 3.7$ to $Re = 59.4$. The low Reynolds number reveals that the flow in the separator unit is laminar.

Flow is simulated by solving the Navier–Stokes equations in velocity-vorticity form. These are the kinematics equation

$$\nabla^2 \mathbf{u} + \nabla \times \boldsymbol{\omega} = 0, \tag{1}$$

and the steady vorticity transport equation

$$(\mathbf{u} \cdot \nabla)\boldsymbol{\omega} = (\boldsymbol{\omega} \cdot \nabla)\mathbf{u} + \nu \nabla^2 \boldsymbol{\omega}, \tag{2}$$

where $\mathbf{u}$ is the velocity field and $\boldsymbol{\omega} = \nabla \times \mathbf{u}$ is the vorticity field.

Boundary conditions for channel flow are: known velocity at inlet, zero velocity flux at outlet, no-slip velocity boundary condition on channel walls. Dirichlet type vorticity boundary conditions are applied on all walls, with vorticity values calculated within the flow kinematics part of the BEM computational algorithm.

A BEM based computational code [21,20] was used to simulate the flow. The system of Eqs. 1 and 2 is solved in a nonlinear loop consisting of three steps. Firstly, calculate boundary vorticity values by solving the kinematics equation by single domain BEM. Secondly, calculate domain velocity values by solving the kinematics equation by subdomain BEM and finally solve vorticity transport equation for domain vorticity values using the boundary values from the solution of the kinematics equation by subdomain BEM.

3.1 Subdomain BEM algorithm

In the subdomain BEM approach the whole domain Ω is divided into subdomains Ω_i, where $\sum \Omega_i = \Omega$. The boundary of each subdomain is denoted by $\partial\Omega_i$. The integral form of the kinematics equation without derivatives of the velocity and vorticity fields takes the following form [for derivation, see Ravnik et al. [18] Eqs. 19–24]:

$$c(\boldsymbol{\vartheta})\mathbf{u}(\boldsymbol{\vartheta}) + \int_{\partial\Omega_i} \mathbf{u}\nabla u^\star \cdot \mathbf{n} d\Gamma = \int_{\partial\Omega_i} \mathbf{u} \times (\mathbf{n} \times \nabla) u^\star d\Gamma + \int_{\Omega_i} (\boldsymbol{\omega} \times \nabla u^\star) d\Omega, \quad (3)$$

where $\mathbf{r}$ is the location point, $\boldsymbol{\vartheta}$ is the collocation point, $\mathbf{n}$ is the unit normal to the boundary and $u^\star = 1/4\pi|\boldsymbol{\vartheta} - \mathbf{r}|$ is the fundamental solution of the Laplace operator. Solution of this equation is used in the second step of the algorithm to obtain domain velocity values.

The integral form of the steady vorticity transport Eq. 2 may be written for the jth component of the vorticity vector as [28]:

$$c(\boldsymbol{\vartheta})\omega_j(\boldsymbol{\vartheta}) + \int_{\partial\Omega_i} \omega_j \nabla u^* \cdot \mathbf{n} d\Gamma = \int_{\partial\Omega_i} u^* q_j d\Gamma + \frac{1}{\nu} \int_{\partial\Omega_i} \mathbf{n} \cdot \left\{ u^* (\mathbf{v}\omega_j - \boldsymbol{\omega} u_j) \right\} d\Gamma - \frac{1}{\nu} \int_{\Omega_i} (\mathbf{u}\omega_j - \boldsymbol{\omega} u_j) \cdot \nabla u^* d\Omega, \quad (4)$$

where ω_j is the jth component of the velocity vector and $\mathbf{q}$ is the vorticity flux vector $q_j = \mathbf{n} \cdot \nabla\omega_j$. Solution of the vorticity transport equations yields domain vorticity values in the final step of the algorithm.

The field functions as well as the products of velocity and vorticity field components are interpolated within elements using shape functions. The mesh elements used in this work are hexahedrons. Quadratic interpolation of function within hexahedron is employed using standard shape functions for a 27 node Lagrangian domain element. On each face of the hexahedron we use discontinuous linear interpolation for flux. All flux nodes are located within boundary elements, none are located at corners and edges—thus the unit normal and the flux value are unambiguously defined in each flux node. In order to calculate the integrals, a Gaussian quadrature algorithm is used.

In order to set up a system of equations the source point is set in all function and flux nodes of all mesh elements. Each element is treated as an individual subdomain, thus a sparse system of equations is obtained. Compatibility boundary conditions are employed between subdomains. The sparse system of equations is solved using least squares based iterative solver.

The flow in a $4.5 \times 0.75 \times 0.75$ mm^3 square cross-section channel was computed using a computational mesh that consisted of $36 \times 12 \times 12$ domain elements having in total 45,625 nodes. The elements were concentrated towards the walls of the channel.

3.2 Solution of the kinematics equation for boundary vorticity by single domain BEM

In order to use the kinematics equation to obtain boundary vorticity values, we rewrite the Eq. 3 into a tangential form by multiplying the system with a normal in the source point:

$$c(\boldsymbol{\vartheta})\mathbf{n}(\boldsymbol{\vartheta}) \times \mathbf{u}(\boldsymbol{\vartheta}) + \mathbf{n}(\boldsymbol{\vartheta}) \times \int_{\partial\Omega} \mathbf{u}\nabla u^\star \cdot \mathbf{n} d\Gamma = \mathbf{n}(\boldsymbol{\vartheta}) \times \int_{\partial\Omega} \mathbf{u} \times (\mathbf{n} \times \nabla) u^\star d\Gamma + \mathbf{n}(\boldsymbol{\vartheta}) \times \int_{\Omega} (\boldsymbol{\omega} \times \nabla u^\star) d\Omega. \quad (5)$$

This approach has been proposed by Škerget and used in $2D$ by Škerget et al. [28] and in 3D by Žunič et al. [32]. We employed the same procedure with the difference of using the second order shape functions, while they used a first order interpolation scheme.

The source point is set in all nodes on the exterior boundary of the domain. This leads to a system of linear equations for boundary vorticity values. The solution of this system is computed in each iteration of the nonlinear solution process until convergence is achieved. Since the system matrix remains unchanged through the whole nonlinear solution procedure, i.e. it does not depend on the flow variables, we perform the LU decomposition on the system matrix before the start of the nonlinear loop. Then, in each iteration of the nonlinear loop, the stored LU decomposition is used to obtain the boundary vorticity values.

4 Magnetic field computation

By adjusting the distance between magnets the strength of the magnetic field is varied. Let this magnetic field strength be denoted by H_0. The external magnetic field magnetizes the wires producing an inhomogeneous magnetic field in the separation channel. Magnetization of the wires and magnetic spheres exhibits nonlinear behaviour, which is shown on $M - H$ curves in Fig. 2. Saturation magnetization of stainless steel wires is 1.38×10^6 A/m and of magnetic spheres 1.6×10^4 A/m.

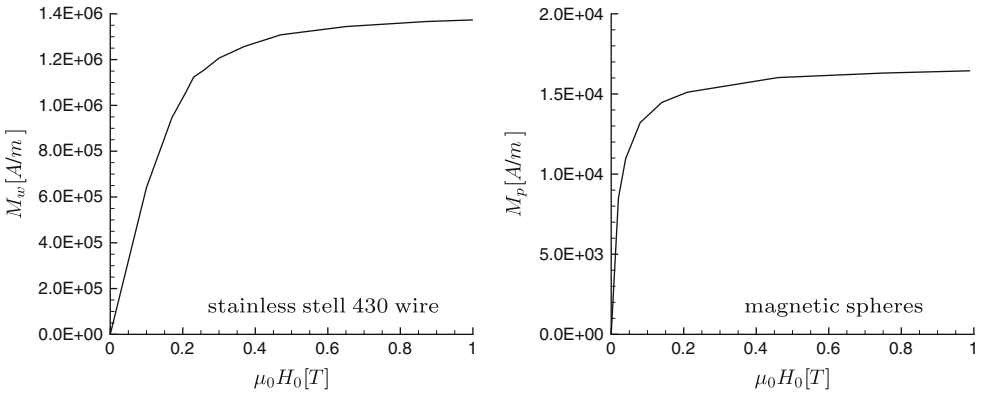

Fig. 2 H–M curve for stainless steel 430 wires (*left*) and magnetic spheres containing 12.45 % magnetite (*right*)

Considering the cylindrical shape of the wires, magnetic field strength $\mathbf{H}$ outside of the wires can be written as [14]:

$$\mathbf{H} = \begin{pmatrix} 0 \\ 0 \\ H_0 \end{pmatrix} - \frac{M_w R^2}{2} \sum_{i=1}^{2} \frac{1}{r_i^4} \begin{pmatrix} 0 \\ 2(y-y_i)(z-z_i) \\ (z-z_i)^2 - (y-y_i)^2 \end{pmatrix}, \tag{6}$$

where M_w is the magnetization of the wires, R the radius of the wires, r_i the distance from the centres of the wires and (y_i, z_i) the location of the centres of the wires. The analytical expression (6) for magnetic field strength $\mathbf{H}$ is used in computation of the Kelvin force acting on particles.

5 Lagrangian particle tracking

Let us consider spherical particles of diameter d_p, mass m_p and density ρ_p. The mass of fluid encompassing the same volume as the particle is denoted by m_f. The equation of motion for small rigid spheres was proposed by Maxey and Riley [10]. Neglecting the aerodynamic lift, time history effects, second order terms and due to small particle size, we may write

$$m_\mathrm{p}\frac{\mathrm{d}\mathbf{v}}{\mathrm{d}t} = (m_\mathrm{p} - m_\mathrm{f})\mathbf{g} + m_\mathrm{f}\frac{D\mathbf{u}}{Dt} - \frac{1}{2}m_\mathrm{f}\left(\frac{d\mathbf{v}}{\mathrm{d}t} - \frac{\mathrm{d}\mathbf{u}}{\mathrm{d}t}\right) - 3\pi d_\mathrm{p}\rho_\mathrm{f}\nu(\mathbf{v}-\mathbf{u}) - 0.1245\mu_0 V_\mathrm{p}\left(\chi_\mathrm{f} - \frac{M_\mathrm{p}}{H}\right)(\mathbf{H}\cdot\nabla)\mathbf{H}. \tag{7}$$

Here $\mathbf{v}$ is the velocity of the particle and $\mathbf{u}$ is the fluid velocity. The terms included in the equation are gravity, buoyancy, pressure gradient term, added mass term, drag (skin friction and form drag) and the magnetic force term. Here, $\mathrm{d}/\mathrm{d}t = \partial/\partial t + (\mathbf{v}\cdot\nabla)$ stands for the time derivative following the particle and $D/Dt = \partial/\partial t + (\mathbf{u}\cdot\nabla)$ the time derivative following the fluid element. The magnetic force term applies to the volumetric fraction of ferromagnetic material (0.1245) and magnetic sphere magnetization M_p. Magnetic susceptibility of water is $\chi_\mathrm{f} = -9\times10^{-6}$.

Equation 7 is rewritten in non-dimensional form with H_0, u_0 and L being the characteristic magnetic field strength, the characteristic fluid velocity scale and characteristic problem length scale, respectively. With $\mathbf{H}\rightarrow\mathbf{H}/H_0$ $\mathbf{u}\rightarrow\mathbf{u}/u_0$, $\mathbf{v}\rightarrow\mathbf{v}/u_0$ and $t\rightarrow tu_0/L$ this renders eventually to

$$\mathbf{a} = \frac{\mathrm{d}\mathbf{v}}{\mathrm{d}t} = \frac{A}{St}\{\mathbf{v}_s + (\mathbf{u}-\mathbf{v})\} + \frac{3}{2}R\frac{\partial\mathbf{u}}{\partial t} + R\{(\mathbf{u}+\frac{1}{2}\mathbf{v})\cdot\nabla\}\mathbf{u} - 0.1245A\frac{\mu_0 H_0^2}{u_0^2\rho_\mathrm{p}}\left(\chi_\mathrm{f} - \frac{M_\mathrm{p}}{H}\right)(\mathbf{H}\cdot\nabla)\mathbf{H}, \tag{8}$$

where the Stokes number is defined as

$$St = \frac{\rho_\mathrm{p} d_\mathrm{p}^2 u_0}{\rho_\mathrm{f} 18\nu L}, \tag{9}$$

the settling velocity is

$$\mathbf{v}_\mathrm{s} = \frac{d_\mathrm{p}^2}{18\nu u_0}\left(\frac{\rho_\mathrm{p}}{\rho_\mathrm{f}} - 1\right)\mathbf{g}, \tag{10}$$

and the parameters R and A are

$$R = \frac{\rho_\mathrm{f}}{\rho_\mathrm{p} + \frac{1}{2}\rho_\mathrm{f}} = 0.4897, \qquad A = \frac{\rho_\mathrm{p}}{\rho_\mathrm{p} + \frac{1}{2}\rho_\mathrm{f}} = 0.7552 \tag{11}$$

The nondimensional magnetic force term is calculated based on magnetic field strength (6) as

$$(\mathbf{H}\cdot\nabla)\mathbf{H} = -\frac{M_w R^2}{2H_0}\sum_{i=1}^{2}\frac{1}{r_i^6} \times \begin{pmatrix} 0 \\ 2(y-y_i)\left(\frac{M_w R^2}{H_0} - 2(y-y_i)^2 + 6(z-z_i)^2\right) \\ 2(z-z_i)\left(\frac{M_w R^2}{H_0} - 6(y-y_i)^2 + 2(z-z_i)^2\right) \end{pmatrix}. \tag{12}$$

With the acceleration of the particle given in Eq. 8 we may solve the particle equation of motion by employing the 4th order Runge-Kutta method [16]. We integrate the following six equations simultaneously:

$$\frac{\mathrm{d}x}{\mathrm{d}t} = v_x, \quad \frac{\mathrm{d}v_x}{\mathrm{d}t} = a_x, \quad \frac{\mathrm{d}y}{\mathrm{d}t} = v_y,$$
$$\frac{\mathrm{d}v_y}{\mathrm{d}t} = a_y, \quad \frac{\mathrm{d}z}{\mathrm{d}t} = v_z, \quad \frac{\mathrm{d}v_z}{\mathrm{d}t} = a_z \tag{13}$$

The unknowns are the particle location (x, y, z) and particle velocity (v_x, v_y, v_z). The initial particle location and velocity must be known. In order to calculate the acceleration contributions on the right hand side, the velocity of the fluid, **u**, has to be calculated at the location of the particle. The solution algorithm described in detail in Ravnik et al. [19] has been used. The developed computer code was parallelized using MPI. Due to consideration of only dilute suspensions the speed up of the parallel code is almost linear. Since particle - particle interactions are not considered, each processor handles its own share of particles and communication between processors is necessary only for writing the results and not during the simulation.

6 Results and discussion

The performance of the separation device is finally determined by its collection efficiency ζ, which is defined by the fraction of magnetic particles that enter the separation channel and become attached to the channel walls. The collection efficiency is expected to depend on the mean flow velocity and on the applied external magnetic field. In order to investigate both effects, two series of numerical experiments have been preformed. Firstly, for mean flow velocity of 5 cm/s the external magnetic field was varied and secondly, for external magnetic field of $\mu_0 H_0 = 0.62$ T the flow velocity was varied.

Table 1 lists mean flow velocities used in simulations along with Reynolds and Stokes number values and time step values. The maximal Reynolds number in simulations was $Re = 59.4$, which means that the flow was steady and laminar. Due to a very small particle diameter (1.7 μm) the particle Stokes numbers are very small, ranging between 10^{-5} and 10^{-6}. The very low Stokes number value means that hydrodynamic forces will force particles to follow the flow almost exactly. The particle settling velocity (10) is $v_s = 0.8\,\mu$m/s, which is very small compared to the height of the channel (0.75 mm), thus the gravitational settling is almost negligible under these circumstances. We can expect that almost an equal number of particles will settle on the top and bottom walls of the channel.

The simulations were run with a time step of $\Delta t = 0.75\,\mu$s for flow with $Re > 10$ and with $\Delta t = 0.55\,\mu$s for $Re = 10$.

Table 1 Mean flow velocities used in simulations along with Reynolds and Stokes number values and time step

Re	u_0 (cm/s)	St ($\times 10^{-6}$)	Δt (μs)
59.36	8	26.1	0.75
37.1	5	16.3	0.75
18.55	2.5	8.15	0.75
10.0	1.35	1.64	0.55

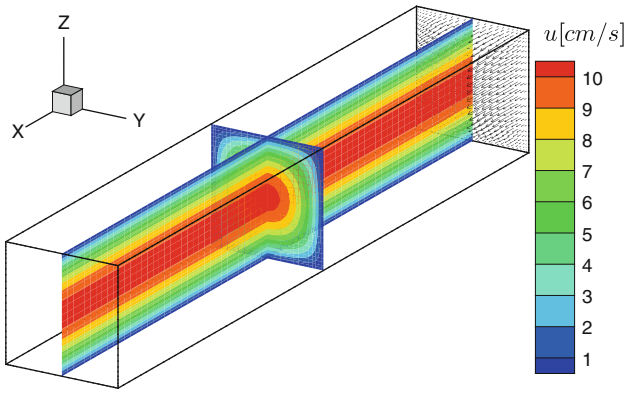

Fig. 3 Flow in a 4.5 mm long section of the separation channel. Figure presents velocity contours and vectors for the case of $u_0 = 5$ cm/s

Simulations ran until all particles either settled on the channel walls or traveled through the whole length of the channel. At the lowest flow rate, this took 5.5 s and ten million time steps. All simulations were ran using 10^4 particles.

At the inflow the particles are homogenously distributed across the whole channel cross-section. As they travel along flow streamlines the magnetic force starts to act on them. The magnetic force is shown with vectors in Fig. 1. The magnetic force pushes the particles towards the centre of the channel and towards the top or bottom wall. The magnetic force is the strongest close to the channel walls and the weakest in the centre of the channel. Flow profiles across the channel reveal the highest flow velocity in the centre of the channel, which diminishes toward zero at channel walls with a parabolic-like profile (Fig. 3). Thus the flow velocity is highest in the area where magnetic forces are weak, while in the vicinity of the walls, the flow is slower and magnetic forces predominate.

As the particles enter the channel, those that are close to the top and bottom walls are immediately drawn to the walls by the strong magnetic force. Particles that enter the channel closer to the centre of the channel, far from both top and bottom walls, are directed towards the centre of the channel and away from the vertical walls. When reaching the centre of the channel, the vertical component of the Kelvin force pulls the particles towards the top and bottom walls. At the entrance of the separation channel, the particles hit the horizontal walls over the whole width of the channel. Further

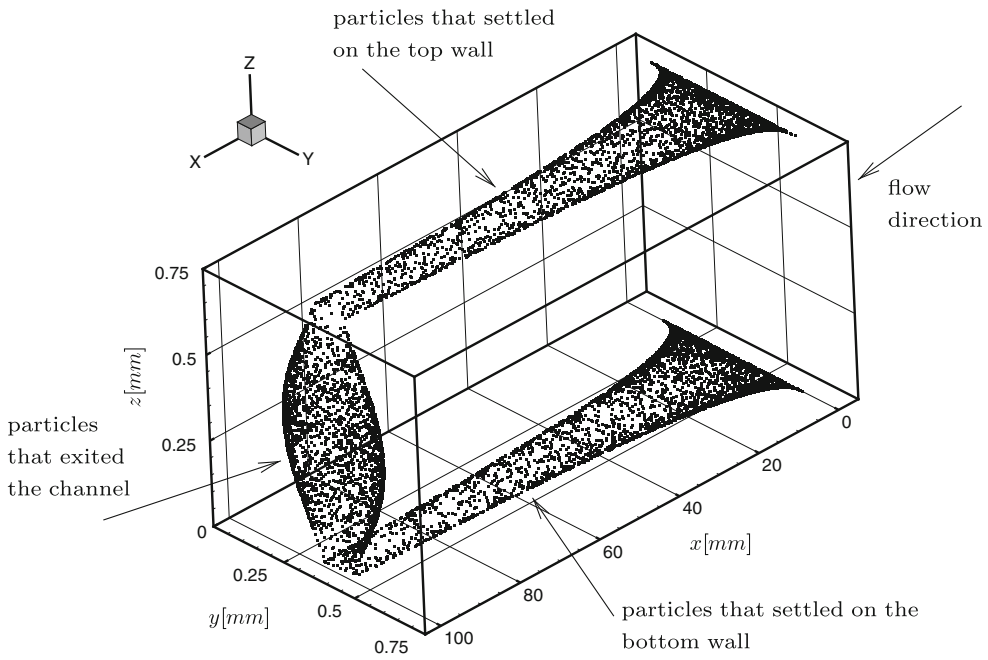

Fig. 4 Final particle positions for the case $u_0 = 5$ cm/s and $\mu_0 H_0 = 0.62$ T

down the channel, due to the horizontal component of the magnetic force, which forces particles towards the centre, particles hit the top and bottom walls close to the centre of the channel. Figure 4 shows the final particle positions for the case of the mean flow velocity of 5 cm/s and external magnetic field of $\mu_0 H_0 = 0.62$ T. Indeed we observe equal distribution of particles that adhered to the top and bottom walls—gravitational settling is negligible (49.5 % of particles settled on the top wall and 50.5 % on the bottom wall). Furthermore at the beginning of the channel particle adhere over the whole width, while further downstream particles are found only in the central area of the channel walls. In the middle of the channel, for example, particles are found only the central 0.2 mm of the top and bottom walls. The particles that exit the channel do so in the central part of the channel, since the flow velocity is the highest there and since the magnetic forces have a component that forces the particles towards the centre.

Figure 5 shows the collection efficiency for the flow velocity of 5 cm/s and various magnetic field densities. In the range of weak magnetic fields, $\mu_0 H_0 \leq 0.15$ T, the collection efficiency increases rapidly with increasing magnetic field density, reaching $\zeta = 0.68$ at $\mu_0 H_0 = 0.15$ T. For stronger magnetic fields saturation is observed, since at $\mu_0 H_0 = 0.62$ T collection efficiency improves only to $\zeta = 0.75$. Saturation was also observed by Chen et al. [3], who made 2D simulations and experiments. Their simulations revealed saturation of collection efficiency at the same magnetic field strengths, but having about 20 % higher values of ζ. Their simulation only considered the central $x-z$ plane

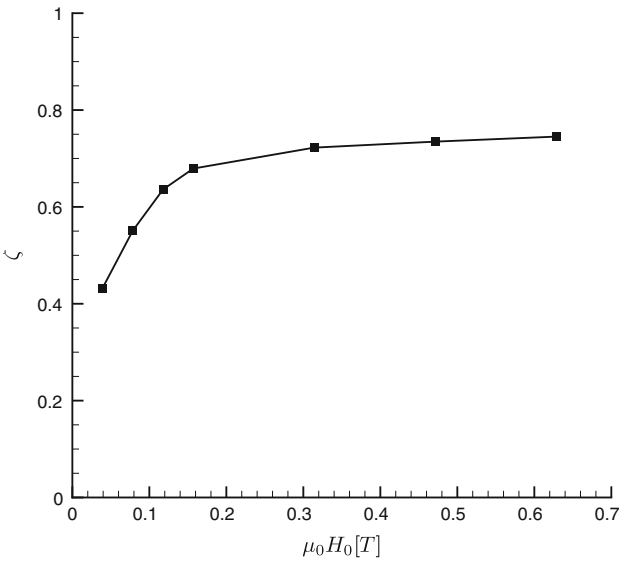

Fig. 5 Collection efficiency ζ versus magnetic field density for $u_0 = 5$ cm/s

of the channel, neglecting the travel of particles towards the centre. It is true that most of the particles adhere to the walls in the central region. The 3D simulation additionally takes into account the travel time of the particles towards the central plane. This is not taken into account in the 2D case, thus it is expected for the 2D simulation to yield higher values of collection efficiencies.

As can be implied from H–M curves (Fig. 2) higher magnetic fields mean stronger magnetization of the wires

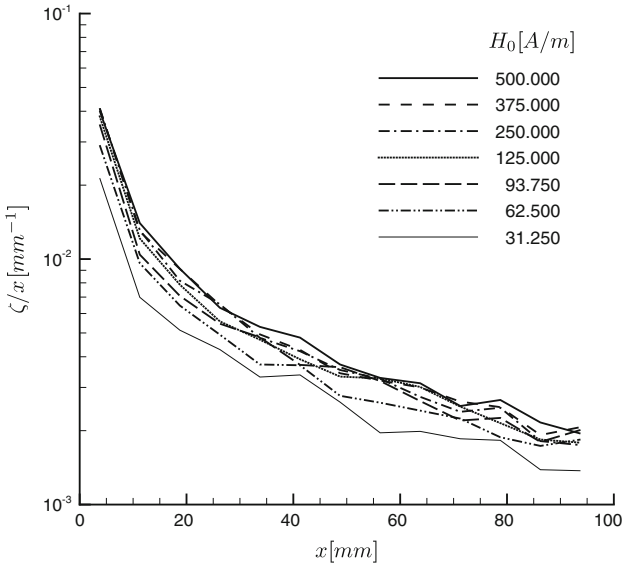

Fig. 6 Collection efficiency per distance ζ/x versus the distance along the separation channel for various h_0 and $u_0 = 5$ cm/s

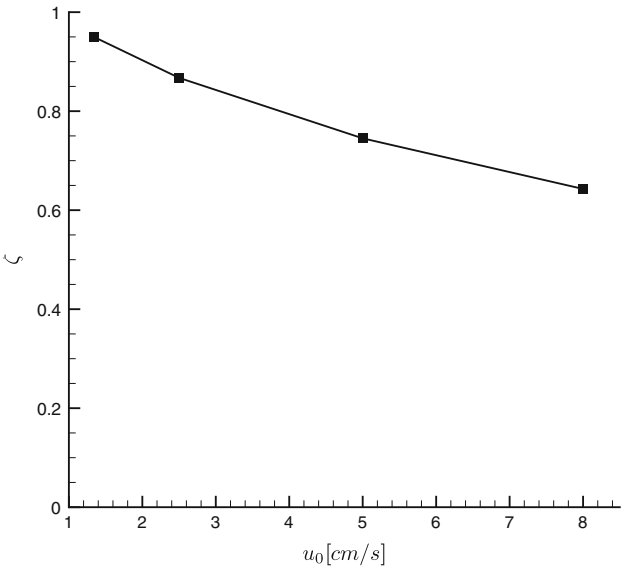

Fig. 7 Collection efficiency ζ versus flow rate for $H_0 = 5 \times 10^5$ A/m, $\mu_0 H_0 = 0.62$ T

and of magnetic particles and thus yields an increase of the collection efficiently of the magnetic separator. However, since magnetization exhibits saturation for high magnetic fields and since stronger magnets mean higher costs and increased weight and safety concerns, strong magnetic field seems unfeasible. The magnetic field strength should be chosen individually with a specific application in mind, considering particle and wire properties and an optimal flow rate.

Next, we investigate collection efficiency per distance ζ/x versus the distance along the separation channel for various external magnetic fields strengths and $u_0 = 5$ cm/s, which is shown in Fig. 6. Collection efficiency per distance is calculated by measuring the number of particles that adhere to the wall at a certain part of the channel divided by the width of that part. It tells us, which parts of the channel are more efficient in terms of collecting the particles and gives an indication of the useful length of the channel. Collection efficiency per distance is the highest at the entrance of the channel, where homogenously distributed particles first undergo the influence of magnetic forces. Further downstream the efficiency drops, since it takes additional time for the particles to move towards the central plane and finally towards the top and bottom walls. Similar behaviour is observed for all magnetic fields, where, as expected, the strongest magnetic field yields the highest collection efficiency.

Figure 7 presents collection efficiency ζ versus flow rate for a constant external magnetic field strength of $\mu_0 H_0 = 0.62$ T. Approximately linear dependence is observed, collection efficiency decreasing with increasing flow velocity. Linear behaviour was also observed by Chen et al. [3]. Exam-

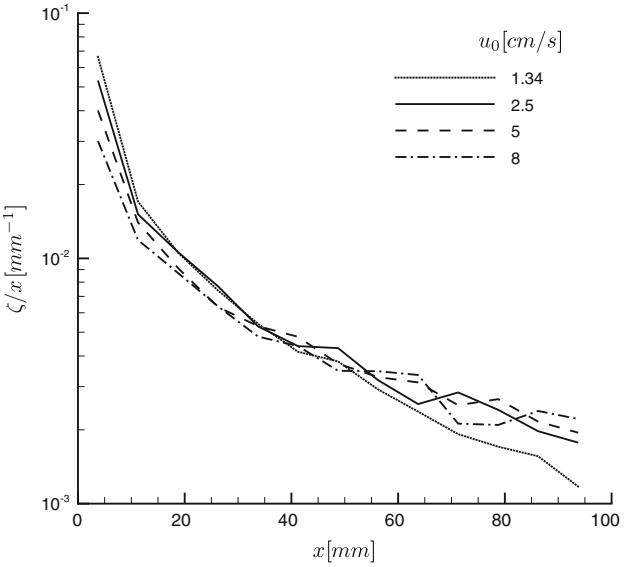

Fig. 8 Collection efficiency per distance ζ/x versus the distance along the separation channel for various u_0 and $H_0 = 5 \times 10^5$ A/m, $\mu_0 H_0 = 0.62$ T

ining collection efficiency per distance ζ/x within the separator in Fig. 8, we observe that low flow velocity yields high collection efficiency at the start of the channel and low collection efficiency at the end of the channel. This leads to a conclusion that the optimal length of the separator channel should be chosen with regard to the flow rate. Separation channel operation at low flow velocity can be shorter and achieve the same collection efficiency as a longer one operating at a higher flow velocity.

7 Conclusions

The BEM was applied to study the motion of magnetic particles in fluid flow under the action of external nonuniform magnetic field. The derived formulation combines the velocity-vorticity resolved Navier–Stokes equations with the Lagrange based particle tracking model, where the one-way coupling with fluid phase was considered. The selected test case of high gradient magnetic separation in a narrow channel was computed in order to test the derived algorithm in computing particles trajectories in channel flow under the influence of hydrodynamic and magnetic forces. The computational case was focused on a HGMS in form of a separation channel with a square cross-section and a high aspect ratio, where magnetic field gradient was caused by two magnetized wires placed on top of and below the bottom of the channel.

The results showed that high collection efficiency is not feasible at high flow velocity and/or at weak magnetic field. Collection efficiency was found to increase with magnetic field strength only up to a certain point, after which saturation occurred. Saturation is caused by the fact that magnetization of wires and magnetic particles also exhibit saturation, thus making the use of very strong external magnets infeasible. Furthermore, we found that the collection efficiency decreases linearly with increasing flow rate. At low flow rate increasing the channel length is inefficient, since the number of collected particles decreases with distance. The final recommendation is to use multiple shorter parallel separation channels, where flow rates can be low, and an external magnetic field just under the saturation regime.

The derived numerical algorithm for the solution of a dilute suspension flow is suitable to combine with a direct BEM based solution of a magnetostatic field problem and consequently to study advanced particle separation devices, such as in magnetic split-flow thin fractionation, under laminar flow conditions. Additionally, the directly resolved vorticity field presents an excellent foundation for including into the computational algorithm also the angular momentum transport, i.e. effect of the flow field on rotation of particles.

References

1. Bozkaya C, Tezer-Sezgin M (2012) A numerical solution of the steady mhd flow through infinite strips with bem. Eng Anal Bound Elem 36(4):591–599. doi:10.1016/j.enganabound.2011.11.005
2. Chen H, Kaminski M, Liu X, Xie Y, Mertz C, Torno M et al (2007) A novel human detoxification system based on nanoscale bioengineering and magnetic separation techniques. Med Hypotheses 68:1071–1079
3. Chen H, Kaminski MD, Rosengart AJ (2008) 2D modeling and preliminary in vitro investigation of a prototype high gradient magnetic separator for biomedical applications. Med Eng Phys 30: 1–8
4. Ditsch A, Lindenmann S, Laibinis PE, Wang D, Hatton TA (2005) High-gradient magnetic separation of magnetic nanoclusters. Ind Eng Chem Res 44:6824–6836
5. Florez W, Power H (2002) DRM multidomain mass conservative interpolation approach for the BEM solution of the two-dimensional Navier–Stokes equations. Comput Math Appl 43(35):457–472. doi:10.1016/S0898-1221(01)00298-X
6. Furlani EP (2006) Analysis of particle transport in a magnetophoretic microsystem. J Appl Phys 99:1–11
7. Giraldo M, Power H, Florez WF (2009) Numerical simulation of the motion and deformation of a non-Newtonian shear-thinning drop suspended in a Newtonian circular Couette flow using DR-BEM. Eng Anal Bound Elem 33(1):93–104. doi:10.1016/j.enganabound.2008.03.003
8. Hatch G, Stelter R (2001) Magnetic design considerations for devices and particles used for biological high-gradient magnetic separation (HGMS) systems. J Magn Magn Mater 225: 262–276
9. Kaminski MD, Rosengart AJ (2005) Detoxification of blood using injectable magnetic nanospheres: a conceptual technology description. J Magn Magn Mater 293:398–403
10. Maxey M, Riley J (1983) Equation of motion for a small rigid sphere in a nonuniform flow. Phys Fluids 26:883–889
11. Moeser GD, Roach KA, Green WH, Hatton TA (2004) High-gradient magnetic separation of coated magnetic nanoparticles. AIChE J 50:2835–2848
12. Nakamura M, Decker K, Chosy J, Comella K, Melnik K, Moore L et al (2001) Separation of a breast cancer cell line from human blood using a quadrupole magnetic flow sorter. Biotechnol Prog 17:1145–1155
13. Pankhurst Q, Connolly J, Jones S, Dobson J (2003) Applications of magnetic nanoparticles in biomedicine. J Phys D 36: R167–R181
14. Peeters H (2006) Analysis and exploitation of field imperfections in magnetic resonance imaging. PhD thesis, Utrecht University
15. Pekas N, Granger M, Tondra M, Popple A, Porter M (2005) Magnetic particle diverter in an integrated microfluidic format. J Magn Magn Mater 293:584–588
16. Press WH, Teukolsky SA, Vetterling WT, Flannery BP (1997) Numerical recipes—the art of scientific computing, 2nd edn, Cambridge University Press, Cambridge
17. Goleman R (2004) Macroscopic model of particles capture by the elliptic cross-section collector in magnetic separator. J Magn Magn Mater 272–276:2348–2349
18. Ravnik J, Škerget L, Hriberšek M (2006) 2D velocity vorticity based LES for the solution of natural convection in a differentially heated enclosure by wavelet transform based BEM and FEM. Eng Anal Bound Elem 30:671–686
19. Ravnik J, Škerget L, Hriberšek M, Žunič Z (2008) Numerical simulation of dilute particle laden flows by wavelet BEM-FEM. Comput Meth Appl Mech Eng 197/6–8:789–805. doi:10.1016/j.cma.2007.09.007
20. Ravnik J, Škerget L, Žunič Z (2008) Velocity-vorticity formulation for 3D natural convection in an inclined enclosure by BEM. Int J Heat Mass Transf 51:4517–4527. doi:10.1016/j.ijheatmasstransfer.2008.01.018
21. Ravnik J, Škerget L, Žunič Z (2009) Combined single domain and subdomain BEM for 3D laminar viscous flow. Eng Anal Bound Elem 33:420–424. doi:10.1016/j.enganabound.2008.06.006
22. Ritter J, Ebner A, Daniel K, Stewart KL (2004) Application of high gradient magnetic separation principles to magnetic drug targeting. J Magn Magn Mater 280:184–201
23. Sellountos E, Sequeira A (2008) A hybrid multi-region BEM / LBIE-RBF velocity-vorticity scheme for the two-dimensional Navier–Stokes equations. CMES Comput Methods Eng Sci 23:127–147
24. Sellountos EJ, Sequeira A (2008) An advanced meshless LBIE/RBF method for solving two-dimensional incompressible fluid flows. Comput Mech 41:617–631

25. Singh H, Laibinis P, Hatton T (2005) Rigid, superparamagnetic chains of permanently linked beads coated with magnetic nanoparticles. Synthesis and rotational dynamics under applied magnetic fields. Langmuir 21:11500–11509
26. Stuart DC, Kleijn C, Kenjeres S (2011) An efficient and robust method for lagrangian magnetic particle tracking in fluid flow simulations on unstructured grids. Comput Fluids 40(1):188–194. doi:10.1016/j.compfluid.2010.09.001
27. Svoboda J, Ross V (1989) Particle capture in the matrix of a magnetic separator. Int J Miner Process 27:75–94
28. Škerget L, Hriberšek M, Žunič Z (2003) Natural convection flows in complex cavities by BEM. Int J Num Methods Heat Fluid 13:720–735
29. Tsutsui H, Ho CM (2009) Cell separation by non-inertial force fields in microfluidic systems. Mech Res Commun 36:92–103
30. Yang J, Park J, Lee J, Cha B, Song Y, Yoon HG, Huh YM, Haam S (2007) Motions of magnetic nanosphere under the magnetic field in the rectangular microchannel. J Magn Magn Mater 317(1-2):34–40. doi:10.1016/j.jmmm.2007.04.008
31. Ying TY, Yiacoumi S, Tsouris C (2000) High-gradient magnetically seeded filtration. Chem Eng Sci 55:1101–1113
32. Žunič Z, Hriberšek M, Škerget L, Ravnik J (2007) 3-D boundary element-finite element method for velocity-vorticity formulation of the Navier-Stokes equations. Eng Anal Bound Elem 31:259–266. doi:10.1016/j.enganabound.2006.09.001